JOURNAL OF AIRCRAFT
Vol. 29, No. 4, July–Aug. 1992

Navier-Stokes Computations on Swept-Tapered Wings, Including Flexibility

Guru P. Guruswamy*
NASA Ames Research Center, Moffett Field, California 94035

A procedure to couple the Navier-Stokes solutions with modal structural equations of motion is presented for computing aeroelastic responses of flexible fighter wings. The Navier-Stokes flow equations are solved by a finite difference scheme with dynamic grids. The coupled aeroelastic equations of motion are solved using the linear-acceleration method. The configuration-adaptive dynamic grids are time-accurately generated using the aeroelastically deformed shape of the wing. The coupled calculations are compared with experiments when available. Effects of flexibility and pitch rate are demonstrated for flows with vortices.

Nomenclature

A = pitch rate of ramp motion
a = speed of sound
b = full-span of the wing
C_p = coefficient of pressure
$\{d\}$ = displacement vector
E, F, G, Q = flux vectors in Cartesian coordinates
e = total energy per unit volume
M, D, K = modal mass, damping and stiffness matrices, respectively
P_r = Prandtl number
p = pressure
$\{q\}$ = generalized displacement vector
Re_c = Reynolds number based on the root chord
S = viscous flux vector
U = flight velocity
u, v, w = velocity components in x, y, and z directions, respectively
x, y, z = Cartesian coordinates
$\{Z\}$ = generalized force vector
α = angle of attack
γ = ratio of specific heats
Δ = difference between upper and lower surface pressures
μ = coefficient of dynamic viscosity
ξ, η, ζ = general curvilinear coordinates
ρ = density
τ = nondimensional time
$[\phi]$ = modal displacement matrix

Subscripts

v = viscous quantities
∞ = freestream quantities

Superscripts

$\hat{}$ = quantities in generalized coordinate system
$\cdot$ = first derivative with respect to time
$\cdot\cdot$ = second derivative with respect to time

Presented as Paper 90-1152 at the AIAA/ASME/ASCE/AHS/ASC 31st Structures, Structural Dynamics and Materials Conference, Long Beach, CA, April 2–4, 1990. Received April 23, 1990; revision received July 2, 1991; accepted for publication July 11, 1991.

*Research Scientist, Applied Computational Fluids Branch. Associate Fellow AIAA.

Introduction

UNDERSTANDING the nature of flows and their interactions with structures is becoming more important than ever for aircraft, particularly for fighters. High performance and maneuverability are playing major roles in the design of fighters. Because of extreme flight conditions, flows over fighters are quite often complex, and are associated with vortices, shock waves, and separation.

The formation of vortices changes the aerodynamic load distribution on a wing. Vortices formed on aircraft have caused several instabilities, such as wing rock[1] for a rigid delta wing and aeroelastic oscillations for a highly swept flexible wing.[2] Such instabilities can severely impair the performance of an aircraft. On the other hand, there are possibilities of using the vortices to control the aircraft at high angles of attack when some of the conventional control techniques are not adequate. Also, it has been claimed that vortical flows associated with rapid, unsteady motions are able to increase the unsteady lift, which can be used for maneuvering the aircraft.[3] The presence of shock waves on wings can reduce the flutter speed and considerably influence the role of active control surfaces. Flow separation can further complicate the above phenomena. All these phenomena are often dominated by viscous effects. For example, the aeroelastic oscillations reported for the highly swept wing in Ref. 2 is a result of the phase-lag effect of viscous dominated vortical flows involving separation. Most of the flows at high angles of attack are dominated by viscous effects.[4] The Navier-Stokes equations are necessary to accurately model these cases dominated by viscous effects.

To date, most of the Navier-Stokes calculations for three-dimensional flows have been restricted to steady[5] and unsteady[4] computations on rigid configurations. For realistic configurations it is necessary to account for the wing flexibility in order to compute flows accurately. The aeroelastic deformation resulting from the flexibility of a wing can considerably change the nature of the flow. Strong interactions between the vortical flows and the structures can lead to sustained aeroelastic oscillations for highly swept wings.[6] Also, it is necessary to include the flexibility for proper correlations of computed data with experiments, particularly with those obtained from flight tests. In order to account for the flexibility of a wing, it is necessary to solve the aerodynamic and aeroelastic equations of motion simultaneously.

In this work, the flow is modeled using the Navier-Stokes equations and is coupled with the aeroelastic equations of

motion. The computer code developed for computing the unsteady aerodynamics and aeroelasticity of aircraft using the Euler/Navier-Stokes equations is referred to as ENSAERO.[7] The flow is solved by time-accurate, finite-difference schemes based on the Beam-Warming algorithm. The capability of the code to compute aeroelastic responses by simultaneously integrating the Euler equations and the modal structural equations of motion, using aeroelastically adaptive dynamic grids, was previously demonstrated in Ref. 7. Recently the capability of ENSAERO was extended to couple solutions from the Navier-Stokes equations with the modal structural equations for laminar flows. The capability of the code to numerically simulate laminar viscous flows on flexible rectangular wings was demonstrated in Ref. 8.

In this work, the capability of the code is further extended to model unsteady turbulent flows about flexible fighter wings. Computations are made for transonic flows and high-angle-of-attack conditions about fighter wings, and the results are compared with available experiments. The formation of vortices and their dynamics on wings are demonstrated, as are the effects of flexibility and pitch rate for wings in unsteady ramp motion.

Aerodynamic Equations and Approximations

The strong conservation-law form of the Navier-Stokes equations is used for shock-capturing purposes. In Cartesian coordinates these equations can be written in nondimensional form as[9]

$$\frac{\partial \boldsymbol{Q}}{\partial t} + \frac{\partial \boldsymbol{E}}{\partial x} + \frac{\partial \boldsymbol{F}}{\partial y} + \frac{\partial \boldsymbol{G}}{\partial z} = \frac{\partial \boldsymbol{E}_v}{\partial x} + \frac{\partial \boldsymbol{F}_v}{\partial y} + \frac{\partial \boldsymbol{G}_v}{\partial z} \tag{1}$$

where

$$\boldsymbol{Q} = \begin{bmatrix} \rho \\ \rho u \\ \rho v \\ \rho w \\ e \end{bmatrix}$$

$$\boldsymbol{E} = \begin{bmatrix} \rho u \\ \rho u^2 + p \\ \rho uv \\ \rho uw \\ u(e + p) \end{bmatrix} \quad \boldsymbol{F} = \begin{bmatrix} \rho v \\ \rho uv \\ \rho v^2 + p \\ \rho vw \\ v(e + p) \end{bmatrix} \quad \boldsymbol{G} = \begin{bmatrix} \rho w \\ \rho uw \\ \rho vw \\ \rho w^2 + p \\ w(e + p) \end{bmatrix}$$

$$\boldsymbol{E}_v = Re_c^{-1} \begin{bmatrix} 0 \\ \tau_{xx} \\ \tau_{yx} \\ \tau_{zx} \\ \beta_x \end{bmatrix} \quad \boldsymbol{F}_v = Re_c^{-1} \begin{bmatrix} 0 \\ \tau_{xy} \\ \tau_{yy} \\ \tau_{zy} \\ \beta_y \end{bmatrix} \quad \boldsymbol{G}_v = Re_c^{-1} \begin{bmatrix} 0 \\ \tau_{xz} \\ \tau_{yz} \\ \tau_{zz} \\ \beta_z \end{bmatrix} \tag{2}$$

with

$$\begin{aligned} \tau_{xx} &= \lambda(u_x + v_y + w_z) + 2\mu u_x \\ \tau_{yy} &= \lambda(u_x + v_y + w_z) + 2\mu v_y \\ \tau_{zz} &= \lambda(u_x + v_y + w_z) + 2\mu w_z \\ \tau_{xy} &= \tau_{yx} = \mu(u_y + v_x) \\ \tau_{xz} &= \tau_{zx} = \mu(u_z + w_x) \\ \tau_{yz} &= \tau_{zy} = \mu(v_z + w_y) \end{aligned}$$

$$\begin{aligned} \beta_x &= \gamma\kappa Pr^{-1}\partial_x e_I + u\tau_{xx} + v\tau_{xy} + w\tau_{xz} \\ \beta_y &= \gamma\kappa Pr^{-1}\partial_y e_I + u\tau_{yx} + v\tau_{yy} + w\tau_{yz} \\ \beta_z &= \gamma\kappa Pr^{-1}\partial_z e_I + u\tau_{zx} + v\tau_{zy} + w\tau_{zz} \\ e_I &= e\rho^{-1} - 0.5(u^2 + v^2 + w^2) \end{aligned} \tag{3}$$

The Cartesian velocity components, u, v, and w are nondimensionalized by a_∞ (the free-stream speed of sound); density ρ is nondimensionalized by ρ_∞ and the total energy per unit volume e is nondimensionalized by $\rho_\infty a_\infty^2$. Pressure can be found from the ideal gas law as

$$p = (\gamma - 1)[e - 0.5\rho(u^2 + v^2 + w^2)] \tag{4}$$

To enhance numerical accuracy and efficiency and to handle boundary conditions more easily, the governing equations are transformed from Cartesian coordinates to general curvilinear coordinates where

$$\begin{aligned} \tau &= t \\ \xi &= \xi(x, y, z, t) \\ \eta &= \eta(x, y, z, t) \\ \zeta &= \zeta(x, y, z, t) \end{aligned} \tag{5}$$

The resulting transformed equations are not much more complicated than the original Cartesian set and can be written in nondimensional form as

$$\frac{\partial}{\partial \tau}\hat{\boldsymbol{Q}} + \frac{\partial}{\partial \xi}(\hat{\boldsymbol{E}} - \hat{\boldsymbol{E}}_v) + \frac{\partial}{\partial \eta}(\hat{\boldsymbol{F}} - \hat{\boldsymbol{F}}_v) + \frac{\partial}{\partial \zeta}(\hat{\boldsymbol{G}} - \hat{\boldsymbol{G}}_v) = 0 \tag{6}$$

where $\hat{}$ indicates the transformed quantities.

In order to solve Eq. (6) for the full flowfield, a very fine grid is required throughout the flowfield. In high-Reynolds-number flows, the viscous effects are confined to a thin layer near surface boundaries. Because of computer storage and speed limitations, in most practical cases there are only enough grid points to resolve the gradients normal to the body by clustering the grid in the normal direction. Resolution along the body is similar to that used in inviscid flow. As a result, even if the full derivatives were retained in the equations, the gradients along the body are not resolved unless the streamwise and circumferential grid spacings are sufficiently small. Hence, for many Navier-Stokes computations, the viscous derivatives along the body are dropped. This leads to the thin-layer Navier-Stokes equations.[10] In this paper, the thin-layer Navier-Stokes form of Eq. (6) is used for modeling the flow.

The thin-layer model requires a body-conforming coordinate system. In our case, the ξ and η directions are along the streamwise and spanwise directions of the wing, respectively,

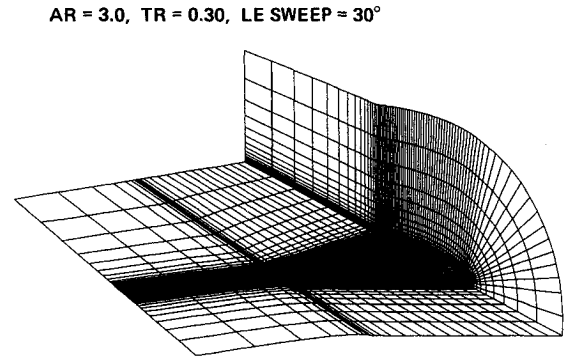

Fig. 1 C–H-type grid topology on a typical fighter wing. (151, 25, and 32 points in x, y, and z directions, respectively).

and the viscous derivatives associated with these directions are dropped, whereas the terms in ζ, normal to the body, are retained and the body surface is mapped onto a constant ζ surface. Thus, Eq. (6) simplifies to

$$\partial_\tau \hat{Q} + \partial_\xi \hat{E} + \partial_\eta \hat{F} + \partial_\zeta \hat{G} = Re^{-1}\partial_\zeta \hat{S} \tag{7}$$

where

$$\hat{S} = J^{-1} \times \begin{bmatrix} 0 \\ \mu(\zeta_x^2 + \zeta_y^2 + \zeta_z^2)u_\zeta + (\mu/3)(\zeta_x u_\zeta + \zeta_y v_\zeta + \zeta_z w_\zeta)\zeta_x \\ \mu(\zeta_x^2 + \zeta_y^2 + \zeta_z^2)v_\zeta + (\mu/3)(\zeta_x u_\zeta + \zeta_y v_\zeta + \zeta_z w_\zeta)\zeta_y \\ \mu(\zeta_x^2 + \zeta_y^2 + \zeta_z^2)w_\zeta + (\mu/3)(\zeta_x u_\zeta + \zeta_y v_\zeta + \zeta_z w_\zeta)\zeta_z \\ \{(\zeta_x^2 + \zeta_y^2 + \zeta_z^2)[0.5\mu(u^2 + v^2 + w^2)_\zeta \\ + \mu Pr^{-1}(\gamma - 1)^{-1}(a^2)_\zeta] + (\mu/3)(\zeta_x u + \zeta_y v + \zeta_z w) \\ \times (\zeta_x u_\zeta + \zeta_y v_\zeta + \zeta_z w_\zeta)\} \end{bmatrix} \tag{8}$$

It should be emphasized that the thin-layer approximation is valid only for high-Reynolds-number flows.

Solution Procedure for Aerodynamic Equations

Several numerical schemes have been developed to solve Eq. (7). In this paper the Pulliam-Chaussee diagonal form[11] of the implicit, approximate-factorization algorithm of Beam and Warming[12] is used. The basic Beam-Warming algorithm is first- or second-order accurate in time and second- or fourth-order accurate in space. The equations are factored (spatially split), which, for a given time iteration, reduces the process to three one-dimensional problems. Because of the second-order central-difference operators employed, the algorithm produces block tridiagonal systems for each spatial dimension. The stability and accuracy of the numerical algorithm is described by Beam and Warming.[12] According to the linear analysis, the numerical scheme is unconditionally stable in two dimensions, but in actual practice time-step limits are encountered because of the nonlinear nature of the equations. However, this limitation is much less stringent than comparable explicit schemes. In three dimensions, the algorithm is

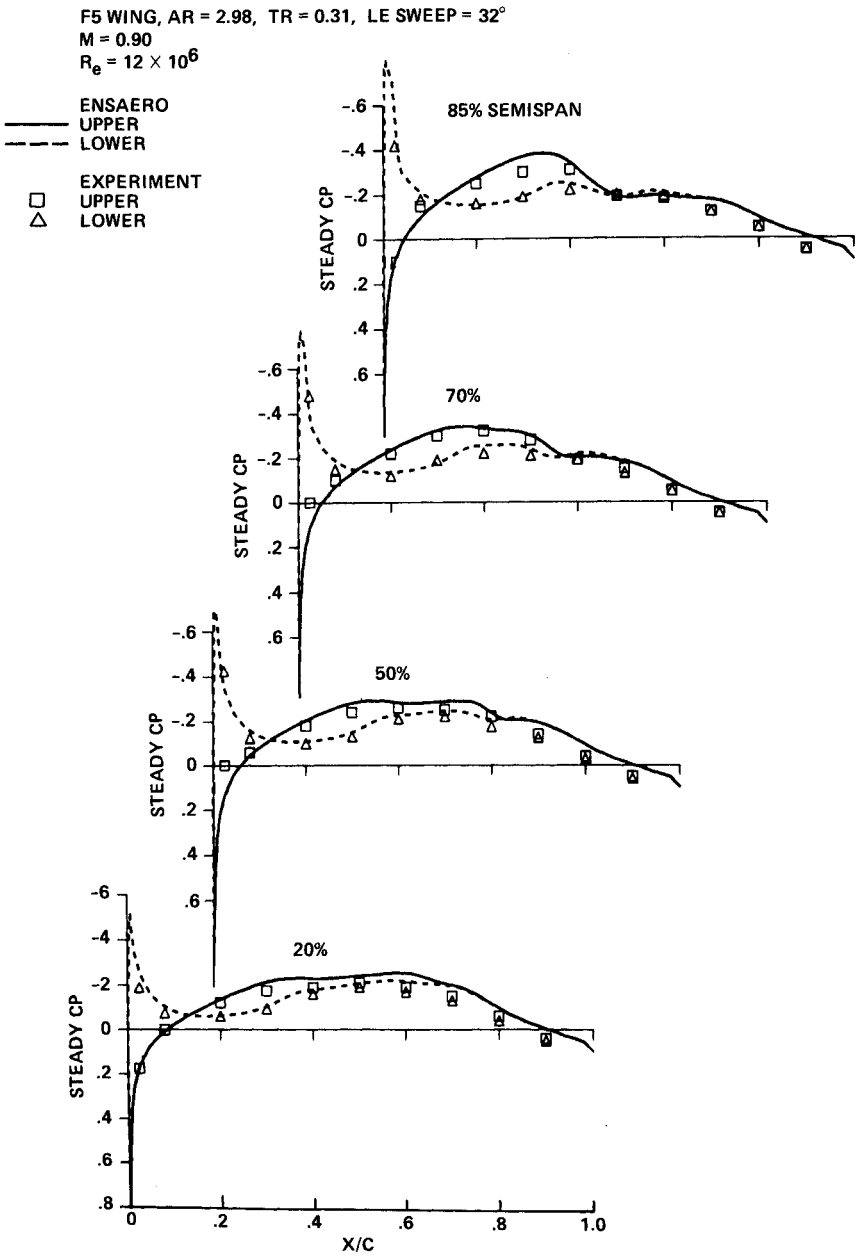

Fig. 2 Comparison of computed steady pressures with experiment for the F-5 wing.

unconditionally unstable, but stability is maintained by the addition of artificial dissipation terms.

Block tridiagonal-matrix inversions constitute the major portion of numerical work associated with the standard Beam-Warming algorithm. Eq. (7) is a coupled set of five equations and, thereby, produce a 5×5 block-tridiagonal structure for the implicit operators. The diagonal version of the standard algorithm due to Pulliam and Chaussee[11] overcomes this difficulty. In this algorithm, rather than inverting block-tridiagonal matrices in each direction, scalar pentadiagonal matrices are inverted. This is computationally more efficient.

The diagonal algorithm is fully implicit for the Euler equations. For the Navier-Stokes equations, the diagonal algorithm treats the viscous terms on the right side of Eq. (7) explicitly. The diagonal algorithm is first-order-accurate in time for both Euler and Navier-Stokes equations. Numerical exercises conducted during this work (and in previous work reported in Ref. 7) showed that the time-step size required to solve Eq. (7) is normally limited by accuracy rather than stability considerations. Therefore, the explicitness of the diagonal algorithm does not influence the computational efficiency when solving the Navier-Stokes equations. Further details about this diagonal scheme can be found in Ref. 11.

For turbulent flow, the coefficient of viscosity appearing in Eq. (8) is modeled using the Baldwin-Lomax algebraic eddy-viscosity model.[13] This isotropic model is used primarily because it is computationally efficient. All viscous computations presented in this paper assume fully turbulent flow, i.e., this approximation is consistent with the high Reynolds-number assumption.

Aeroelastic Equations of Motion

The governing aeroelastic equations of motion of a flexible wing are solved using the Rayleigh-Ritz method.[14] In this method, the resulting aeroelastic displacements at any time are expressed as a function of a finite set of assumed modes. The contribution of each assumed mode to the total motion is derived by Lagrange's equation. Furthermore, it is assumed that the deformation of the continuous wing structure can be represented by deflections at a set of discrete points. This assumption facilitates the use of discrete structural data. These can be generated from a finite-element analysis or from experimental influence-coefficient measurements. In this study, the finite-element method is used to obtain the modal data.

It is assumed that the deformed shape of the wing can be represented by a set of discrete displacements at selected nodes. From the modal analysis, the displacement vector $\{d\}$ can be expressed as

$$\{d\} = [\phi]\{q\} \tag{9}$$

where $[\phi]$ is the modal matrix and $\{q\}$ is the generalized displacement vector. The final matrix form of the aeroelastic equations of motion is

$$[M]\{\ddot{q}\} + [D]\{\dot{q}\} + [K]\{q\} = \{Z\} \tag{10}$$

where $[M]$, $[D]$, and $[K]$ are the modal mass, damping, and stiffness matrices, respectively; $\{Z\}$ is the aerodynamic force vector defined as $(\frac{1}{2})\rho U_\infty^2[\phi]^T[L]\{\Delta C_p\}$; and $[L]$ is the diagonal area matrix of the aerodynamic control points.

The aeroelastic matrix equation of motion, Eq. (10), is solved by a numerical integration technique based on the linear-acceleration method.[15]

Aeroelastic-Configuration-Adaptive Grids

One of the major problems in computational aerodynamics using the Euler/Navier-Stokes equations lies in the area of grid generation. For the case of steady flows, advanced techniques such as zonal grids[5] are being used for full aircraft. Such grid-generation techniques for aeroelastic calculations that involve moving components are in an early stage of development.[16] The effects of the aeroelastic-configuration-adaptive dynamic grids on the stability and accuracy of the numerical schemes are yet to be studied in detail.

This work developed an analytical grid-generation technique for aeroelastic applications. The scheme satisfies the general requirements of a grid required for finite-difference schemes used in the analysis. Some of the requirements are: 1) the grid lines intersect normal to the wing surface in the chordwise direction; 2) the grid cells are smoothly stretched away from the wing surface; 3) the outer boundaries are located far from the wing to minimize the effect of boundary reflections; and 4) the grids adapt to the deformed wing position at each time step.

The computational grids used in this study have a C–H topology, as shown in Fig. 1 for a typical fighter wing. The grid deforms to remain coincident with a wing surface as it deflects, while the outer boundary of the grid is fixed in space. At the end of each time-step, the deformed shape of the wing is computed using Eq. (9). The ξ and η grid distributions on the grid surface corresponding to the wing surface (ζ grid index = 1) are obtained from previously assumed distributions. These distributions are selected to satisfy the general requirements of a grid for accurate computations. In this work, the grid in the ξ direction is selected so that the grid spacing is small near the wing and stretches exponentially to the outer boundaries. The grid near the leading edge is made finer than the rest of the wing in order to model the geometry accurately. In the spanwise direction, a uniformly distributed grid spacing is used on the wing. To model the wing tip, a finer grid spacing is used. Away from the wing tip, the η grid spacing stretches exponentially. The ζ grid spacing is computed at each time step using the deformed shape of the wing computed using Eq. (9). The ζ grid lines start normal to the surface in the chordwise direction and their spacing stretches exponentially to a fixed outer boundary. To prevent the outer boundaries from moving, the grid is sheared in the ζ direction. The metrics required in the computational domain are computed using the following relations:

$$\begin{aligned} \xi_t &= -x_\tau\xi_x - y_\tau\xi_y - z_\tau\xi_z \\ \eta_t &= -x_\tau\eta_x - y_\tau\eta_y - z_\tau\eta_z \\ \zeta_t &= -x_\tau\zeta_x - y_\tau\zeta_y - z_\tau\zeta_z \end{aligned} \tag{11}$$

The grid velocities x_τ, y_τ, and z_τ required in Eq. (11) are computed using the grids at new and old time levels. This adaptive grid generation scheme is incorporated in ENSAERO. The ability of this scheme to compute accurate aeroelastic responses has been demonstrated in Ref. 7.

Computational efficiency and robustness of the solution method are important for computationally intensive aero-

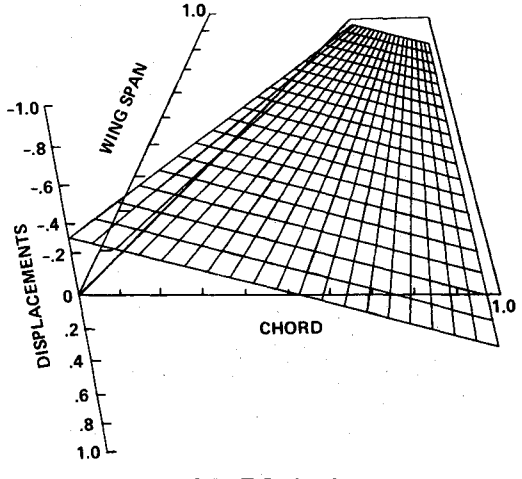

Fig. 3 Unsteady motion of the F-5 wing for unsteady computations.

elastic calculations with configuration-adaptive grids. The diagonal algorithm used in the present study computes time-accurate calculations in a geometrically nonconservative fashion. Geometric conservation can improve the accuracy of the results for moving grids. However, earlier studies have shown that satisfying geometric conservation has little effect on the solutions associated with the moving grids.[17] The time steps used for Navier-Stokes calculations are typically small enough that the error from geometric nonconservation is negligible for most practical purposes. The validation of computed results with experiments reported in this paper and Ref. 16 further support the use of the diagonal scheme for computations associated with moving grids. In order to maintain the efficiency and robustness of the diagonal scheme, the present time-accurate computations are made without geometric conservativeness.

Results

In this work, computations are made for typical fighter-type wings. All computations are made using a C–H-type grid shown in Fig. 1. The grid has 151, 25, and 32 points in the streamwise, spanwise, and normal directions, respectively. The grid spacing in the direction normal ζ to the surface of the wing is of the order 10^{-5} times the chord length. The minimum grid spacing in the ξ direction on the wing surface is of the order 10^{-3} of the chord length. Seventeen spanwise stations are used on the surface of the wing. The distribution of the grid in the spanwise direction is selected such that the spacing is uniform over most of the wing and becomes finer as it approaches the tip. The main objective of this work is to capture most of the flow details in the streamwise and the normal directions. Although the present grid is adequate to model the spanwise three-dimensional effects, it is not designed to capture details of the flow over the tip. From numerical experiments, it is found that this grid spacing is adequate to model turbulent flows including shock waves and vortices on the wing.

All computations are made on CRAY-YMP832 computers available at Ames and NAS (Numerical Aerodynamic Simulation). The current version of ENSAERO runs at 130 MFLOPS (million floating point operations per second). The central processing unit (CPU) time per time step per grid point is 15×10^{-6} and the memory required per grid point is about 30 words with the use of secondary storage, solid state device (SSD).

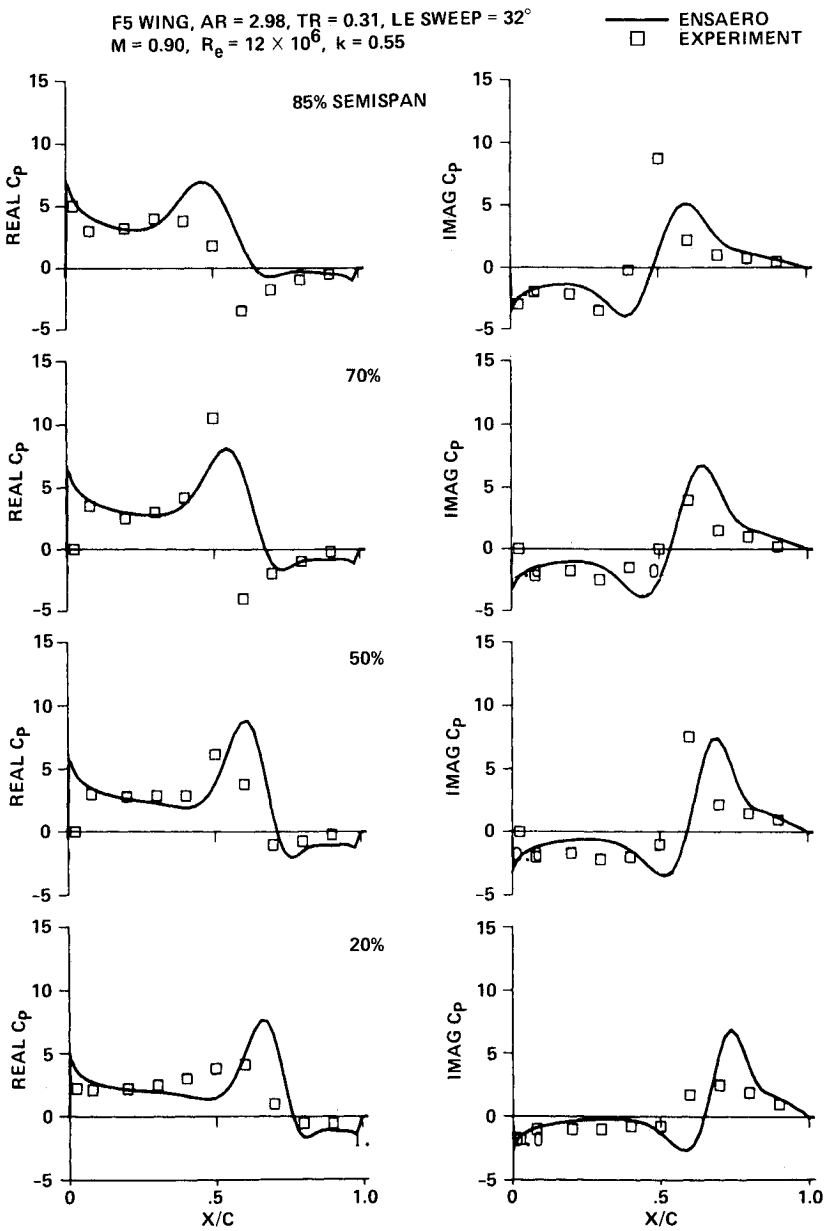

Fig. 4 Comparison of computed unsteady upper surface pressures with experiment for the F-5 wing at M_∞ = 0.90.

Steady Pressures

Steady-state computations are made on the F-5 wing of aspect ratio 2.98 and taper ratio 0.31 to validate the code. The leading-edge sweep angle is 32 deg. For this wing, wind-tunnel data are available from an experiment conducted by Tijdeman et al.[18] at the National Aeronautical Laboratory of the Netherlands (NLR). Figure 2 shows the computed and measured steady pressures at $M_\infty = 0.90$, $\alpha = 0.0$ deg, and Re_c (Reynolds number based on the root chord) $= 12.0 \times 10^6$. The computed steady pressures compare well with the experimental data for all span stations. Slight discrepancies near the leading edge can be attributed to the grid resolution. It is noted that the F-5 wing has a nose that droops down and it requires a very fine grid to capture complete details of the flow. Because the main objective of this work was to design a grid suitable for unsteady flows, it was beyond the scope of the current work to concentrate grid near the nose. This computation verifies the suitability of the grid to make computations on fighter-type wings.

Unsteady Computations on Oscillating Rigid Wing

Time accuracy of the computed results is important for aeroelastic applications. One conclusive way of verifying the time accuracy is by computing flows over oscillating wings and comparing unsteady pressure results with the experiment. In this case, there is a definite reference motion of the wing to verify the time accuracy. This procedure is more exact than just comparing the time-averaged pressures of arbitrary motions. In this section, computations are made on the F-5 wing oscillating in a pitching mode.

Figure 3 shows the modal motion used in the wind tunnel experiment.[18] The wing is pitching about an axis located at the 50% root chord and the pitching axis is normal to the wing root. Computations were made for subsonic $M_\infty = 0.80$ and transonic $M_\infty = 0.90$ Mach numbers at $Re_c = 12.0 \times 10^6$ and a mean angle attack of zero. The comparisons between computed and experimental results are excellent for $M_\infty = 0.80$. Figure 4 shows plots of the upper surface unsteady pressures at four span stations computed by the Navier-Stokes

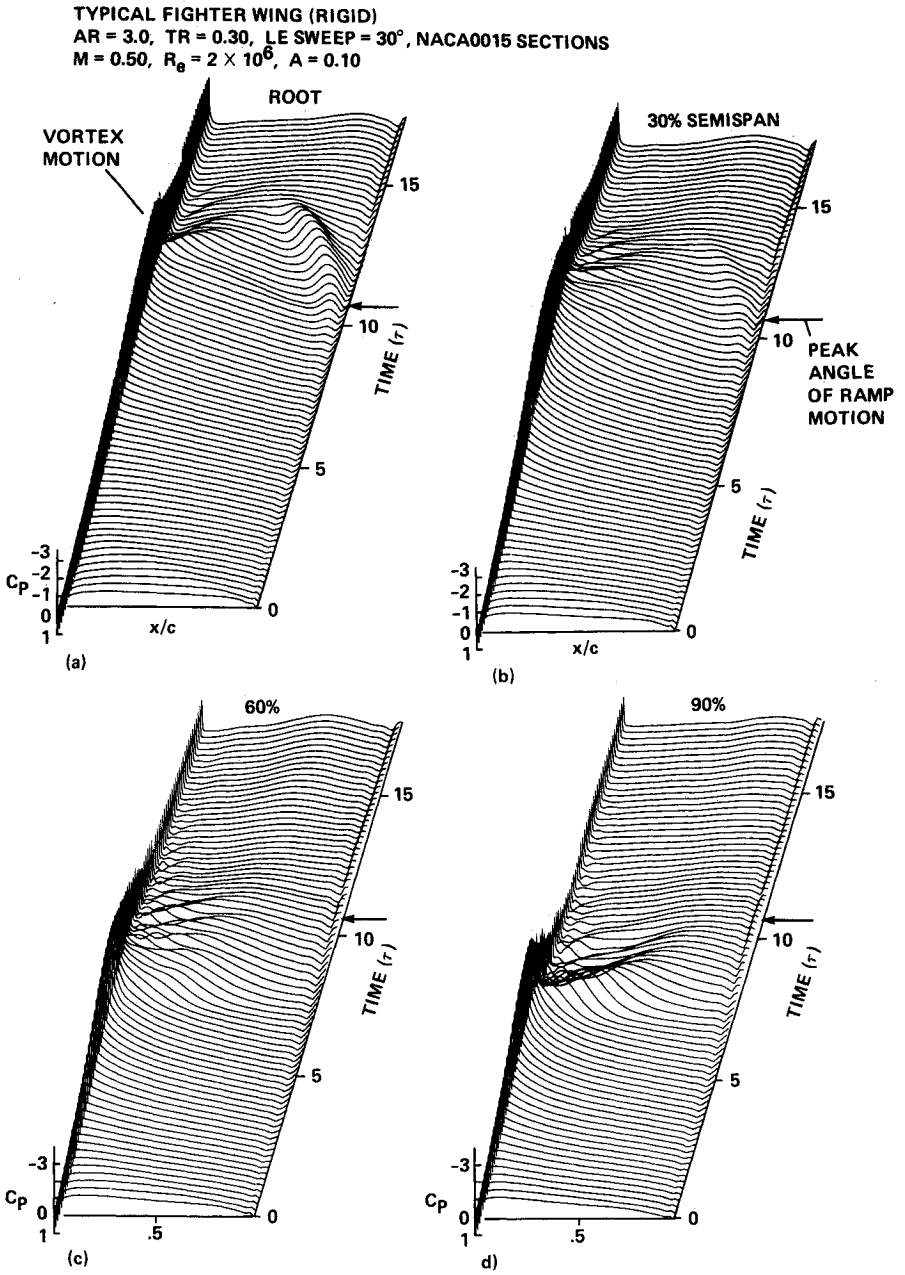

Fig. 5 Unsteady upper surface pressure responses of fighter wing in ramp motion: a) root, b) 30%, c) 60%, and d) 90% sections.

equations and from the NLR experiments at $M_\infty = 0.90$. These results were obtained by harmonically oscillating the wing in a sinusoidal motion at a frequency of 40 Hz with an amplitude of 0.11 deg as it was done in the experiment. Unsteady pressure results from the code were obtained by forcing the wing to undergo a sinusoidal modal motion for three cycles with 1440 time steps per cycle, during which time the transients disappeared and a periodic response was obtained. From numerical experiments it was found that 1440 time steps per cycle were adequate to compute unsteady pressures accurately. The results for the third cycle are shown.

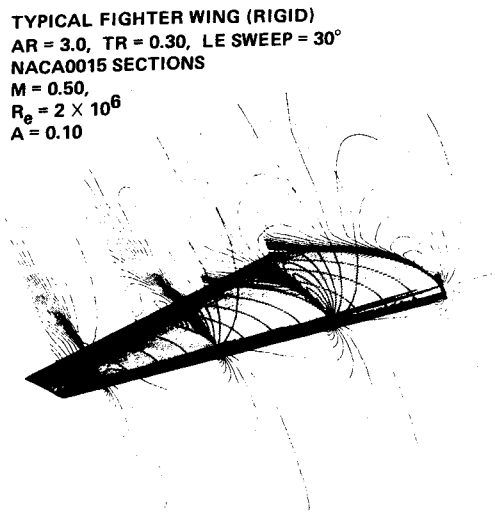

Fig. 6 Velocity contours in freestream direction over the fighter wing at 30-deg ramp angle.

At $M_\infty = 0.80$, where the flow is subsonic, both the real and imaginary parts of the unsteady pressure compare well with the experiment for all spanwise stations. At $M_\infty = 0.90$, where the flow is transonic, the comparisons shown in Fig. 4 are good except near the root and tip. Discrepancies near the root may be due to the wall viscous effects, which are not accounted for in this analysis. A greater number of spanwise stations than are currently used would further improve the solution near the tip. In general, the computed shock wave is slightly downstream of the measured one. These favorable comparisons with the experiment demonstrate the time-accuracy of the present computations.

Unsteady Computations on Wings in Ramp Motion

In this section, ENSAERO is demonstrated to compute flow over a typical fighter-wing pitching from $\alpha = 0.0$ to 30.0 deg in a ramp motion. The wing selected is of aspect ratio of 3.0, taper ratio of 0.30 and leading-edge sweep angle of 30 deg with NACA0015 sections. Computations are made on both rigid and flexible configurations. All computations for both the rigid and flexible wings are made for $M_\infty = 0.50$ and $Re_c = 2.0 \times 10^6$, using a time-step size of 8.4×10^{-3}. From numerical experiments, it was found that the time-step size used is adequate to obtain a stable and accurate unsteady solution.

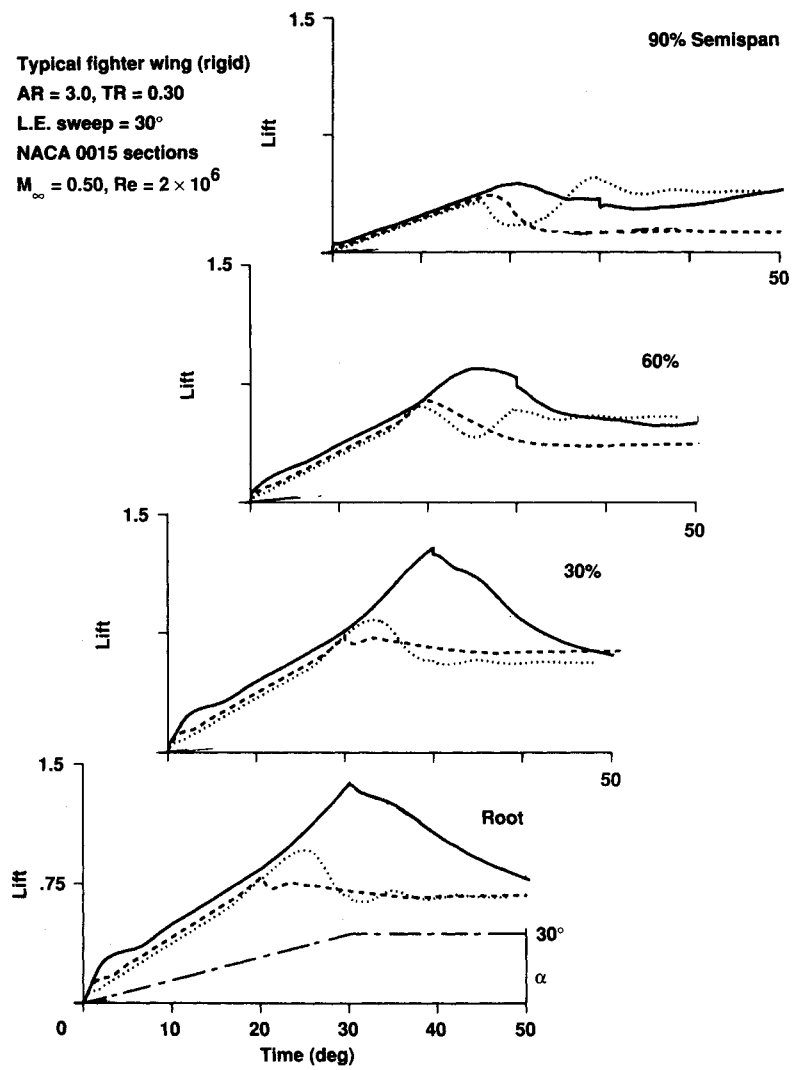

Fig. 7 Effect of pitch rates on lift responses of a fighter wing in ramp motion.

Rigid Wing

For the rigid wing, computations were made at three pitch rates, A of 0.10, 0.050, and 0.025. The pitch rate A is defined as $\dot{\alpha}c/U_\infty$ where α is in radians. Figure 5 shows computed responses of upper surface unsteady pressures for the rigid wing undergoing a ramp motion from $\alpha = 0.0$ to 30 deg at a pitch rate of 0.1. For this pitch rate, the wing reaches $\alpha =$ 30 deg at a nondimensional time of 10.47 as indicated by the arrow in Fig. 5. Chordwise pressure histories for spanwise stations located at $2y/b = 0.0$, 0.3, 0.60, and 0.90 are shown in Figs. 5a–d, respectively. The unsteady computations are started from a converged steady state solution at $\alpha = 0.0$ deg. Figure 5 shows the vortex wing interaction due to initiation, development and convection of the leading edge vortex using three-dimensional pressure topologies plotted at four span stations. The results in Fig. 5 show the dynamics of vortex development. As the wing is pitched toward the maximum angle of attack, a rapid pressure decrease (increasing suction peak) occurs over the leading edge, which signals the formation of a leading-edge vortex. This vortex starts moving downstream rapidly after the wing has reached a certain angle of attack. The vortex motion is highly three dimensional. The vortex core starts moving downstream earlier for span stations closer to the tip. Also it is observed that the tip stall occurs before the root stall. The velocity contours and the location of the vortex core when the wing has reached the maximum ramp angle of 30 deg is shown in Fig. 6. From this, it can be seen that the contours are dissipated near the tip due to the vortex stall whereas a strong vortex is still present on the wing near the root section. Flow is more separated near the tip than near the root. A similar phenomenon has been observed in an experimental study for a rectangular wing at a low Mach number.[19] This computation requires about 5 h of CPU time on CRAY-YMP832 computer.

One area where unsteady vortical flows play an important role is in increasing the dynamic lift. From earlier studies[3] on airfoils, it has been observed that the dynamic lift can be increased by increasing the pitch rates. It is expected that such increases in the dynamic lift can be used in maneuvering an aircraft.[3] Because the dynamic lift is an unsteady phenomenon and is associated with the presence of vortices, it is important to model it accurately. The present computational tool was used to investigate dynamic lift over fighter wings, including the wing flexibility. Computations are made for the rigid fighter wing for pitch rates $A = 0.05$ and 0.025, and the results are

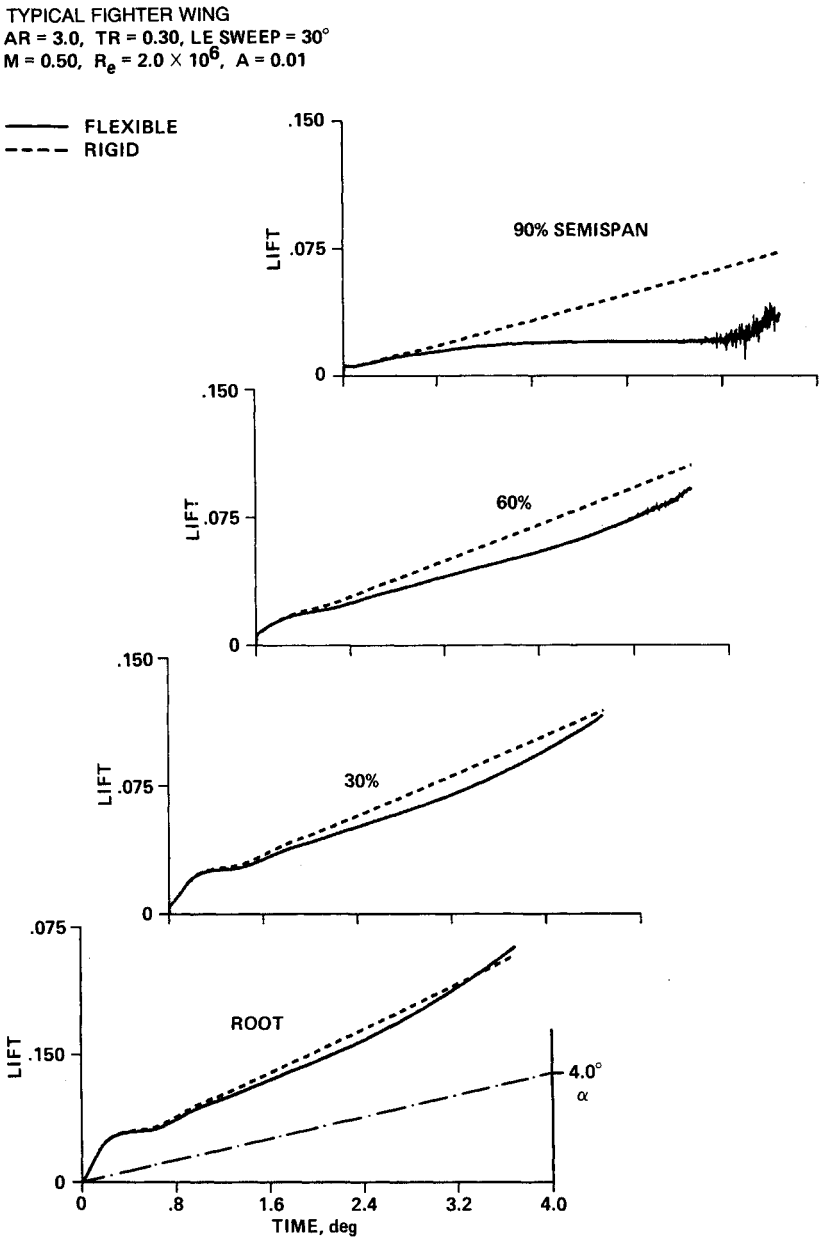

Fig. 8 Effect of wing flexibility on lift responses of a fighter wing in ramp motion.

compared with those obtained earlier for $A = 0.10$. The unsteady lift is plotted against time in degrees in Fig. 7. Thus, the wing reaches the maximum value $\alpha = 30$ deg at t (in degrees) = 30. For all pitch rates, the stall occurs at the wing tip before it occurs at the root section. The increase in the dynamic lift at the higher pitch rates can be seen in Fig. 7.

Flexible Wing

As stated in the introduction, it is important to account for the flexibility of the wing. Significant details of physics may be lost if the wing flexibility is neglected. In order to illustrate the importance of the wing flexibility, computations are made on a flexible configuration of the fighter wing. The structural properties of the flexible wing are modeled using the first bending, first torsional, second bending, and second torsional modes with frequencies of 7.94, 14.78, 24.99, and 32.06 Hz, respectively. These modes and frequencies represent the structural properties of a typical fighter wing. Aeroelastic computations are made at a dynamic pressure of 0.5 psi.

Computations were made for the flexible wing undergoing a ramp motion with a pitch rate of 0.01 and results are compared with the corresponding rigid wing. Figure 8 shows the unsteady lifts for both rigid and flexible wings. When the ramp angle has reached about 3.0 deg, the flow on the flexible wing becomes unsteady because of flow separation that starts near the wing tip. This qualitatively looks like an onset of buffet. On the other hand, the flow is fully attached for the rigid wing. Computation on the flexible wing could not be continued after 3.5 deg due to numerical instability. This numerical instability is originated from the turbulence model. The Baldwin-Lomax turbulence model used in the present study is based on the steady-state equations. For moderate unsteady flows the steady-state turbulence model can be used under quasisteady assumptions. In the present case, the flow is highly unsteady with a frequency of about 800 Hz and, therefore, numerical instability occurs in the turbulence model. This strong unsteadiness associated with flow separation and structural oscillations caused numerical instability in the turbulence model. This was verified by computing the same ramp motion for laminar flows that did not cause any numerical instability. However, numerically efficient unsteady turbulence models are not now available. At Ames Research Center, work is initiated to develop a numerically efficient unsteady turbulence model.

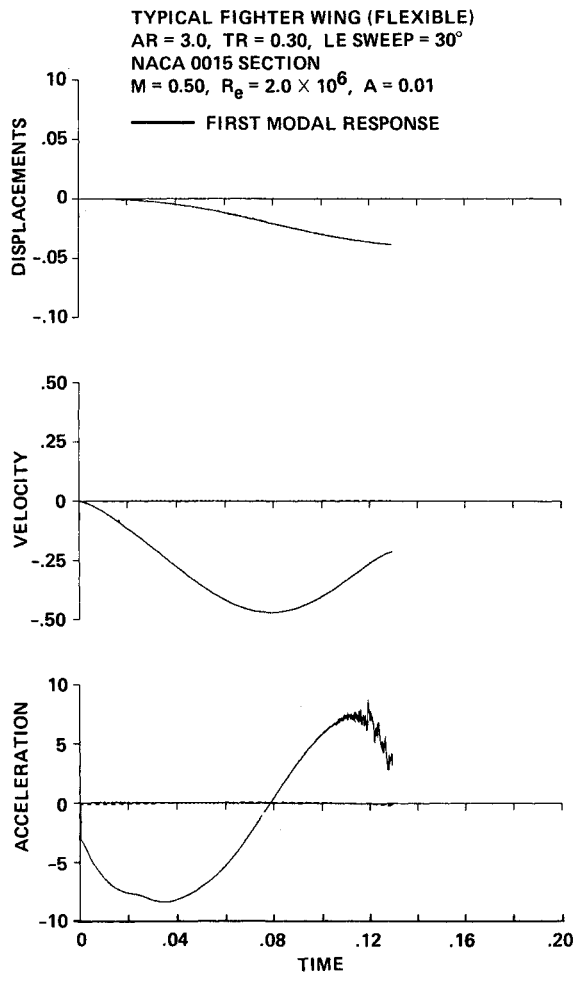

Fig. 9 First modal response of a typical fighter wing.

Unsteady oscillations due to flow separation can be further visualized by studying the modal responses. The wing response was dominated by the first mode. Figure 9 shows the displacement, velocity, and acceleration responses of the first generalized coordinate $q(1)$ of Eq. (10). The effect of the flow unsteadiness due to flow separation can be seen clearly on the acceleration response. It is noted that the flow becomes unsteady only for the flexible wing due to the strong interactions between fluids and structures. The unsteadiness of the flow is reduced as the wing becomes more stiff. This computation illustrates the need to account for the flexibility of the wing.

Summary

In this work coupled solutions of the time-accurate three-dimensional Navier-Stokes equations and those of the modal structural equations of motion has been demonstrated for fighter wings. The time-accurate Navier-Stokes solutions are valid for laminar and turbulent flows, and permit computation of aeroelastic phenomena driven by viscous phenomena that cannot be predicted using either potential or Euler solutions.

Computations on oscillating wings demonstrate that the present procedure can accurately compute transonic flows with moving shock waves. Computations on the rigid wing in ramp motion illustrate the dynamics of vortical flows. For fighter wings at the flow conditions considered here, the vortex has strong spanwise effects and is strongly dependent on pitch rates. The vortex stall occurs earlier in ramp motion near the tip than near the root. Fluids-structural interaction plays an important role on the response. In the present study, the wing flexibility coupled with flow separation caused high-frequency oscillations in the response. The onset of buffet seems to have been predicted by present computations, however, quantitative validation will require further study using an unsteady turbulence model.

References

[1]Nguyen, L. T., Yip, L. P., and Chambers, J. R., "Self-Induced Wing Rock Oscillations of Slender Delta Wings," AIAA Paper 81-1883, Orlando, FL, Aug. 1981.

[2]Dobbs, S. K., and Miller, G. D., "Self-Induced Oscillation Wind Tunnel Test of a Variable Sweep Wing," AIAA Paper 85-0739, Orlando, FL, April 1985.

[3]Mabey, D. G., "On the Prospects for Increasing Dynamic Lift," *Aeronautical Journal*, March 1988, pp. 95–105.

[4]Cummings, R. M., Schiff, L. B., Rizk, Y. M., and Chaderjian, N. C., "Navier-Stokes Predictions of the Flowfield Around the F-18 (HARV) Wing and Fuselage at Large Incidence," AIAA Paper 89-0099, Reno, NV, Jan. 1990.

[5]Flores, J., Chaderjian, N., and Sorenson, R., "The Numerical Simulation of Transonic Separated Flow About the Complete F-16A," AIAA Paper 88-2506, Williamsburg, VA, June 1988.

[6]Guruswamy, G. P., Goorjian, P. M., Ide, H., and Miller, G. D., "Transonic Aeroelastic Analysis of the B-1 Wing," *Journal of Aircraft*, Vol. 23, No. 7, 1986, pp. 547–553.

[7]Guruswamy, G. P., "Time-Accurate Unsteady Aerodynamic and Aeroelastic Calculations of Wings Using Euler Equations," *AIAA Journal*, Vol. 28, No. 3, 1990, pp. 461–469.

[8]Guruswamy, G. P., "Vortical Flow Computations on Swept Flexible Wings Using Navier-Stokes Equations," *AIAA Journal*, Vol. 28, No. 12, 1990, pp. 2077–2084.

[9]Peyret, R., and Viviand, H., "Computation of Viscous Compressible Flows Based on Navier-Stokes Equations," AGARD AG-212, 1975.

[10]Pulliam, T. H., and Steger, J. L., "Implicit Finite-Difference Simulations of Three Dimensional Compressible Flow," *AIAA Journal*, Vol. 18, No. 1, 1980, pp. 159–167.

[11]Pulliam, T. H., and Chaussee, D. S., "A Diagonal Form of an Implicit Approximate Factorization Algorithm," *Journal of Computational Physics*, Vol. 39, No. 2, 1981, pp. 347–363.

[12]Beam, R., and Warming, R. F., "An Implicit Finite-Difference Algorithm for Hyperbolic Systems in Conservation Law Form," *Journal of Computational Physics*, Vol. 22, No. 9, 1976, pp. 87–110.

[13]Baldwin, B. S., and Lomax, H., "Thin-Layer Approximation and Algebraic Model for Separated Turbulent Flows," AIAA Paper 78-257, Huntsville, AL, 1978.

[14]Bisplinghoff, R. L., Ashley, H., and Halfman, R. L., *Aeroelasticity*, Addison Wesley, Reading, MA, 1957.

[15]Guruswamy, P., and Yang, T. Y., "Aeroelastic Time Response Analysis of Thin Airfoils by Transonic Code LTRAN2," *Computers & Fluids*, Vol. 9, No. 4, 1980, pp. 409–425.

[16]Chaderjian, N., and Guruswamy, G. P., "Unsteady Transonic Navier-Stokes Computations for an Oscillating Wing Using Single and Multiple Zones," AIAA Paper 90-0313, Reno, NV, Jan. 1990.

[17]Huff, D. L., "Numerical Simulations of Unsteady, Viscous, Transonic Flow Over Isolated and Cascaded Airfoils Using a Deforming Grid," AIAA Paper 87-1316, Honolulu, HI, June 1987.

[18]Tijdeman, J., van Nunen, J. W. G., Kraan, A. N., Persoon, A. J., Poestkoke, R., Roos, R., Schippers, P., and Siebert, C. M., "Transonic Wind Tunnel Tests on an Oscillating Wing with External Strores; Part II—The Clean Wing," Air Force Flight Dynamics Laboratory TR-78-194, March, 1979.

[19]Robinson, M. C., and Wissler, J. B., "Unsteady Surface Pressure Measurements on a Pitching Rectangular Wing," AIAA Paper 88-0328, Reno, NV, Jan. 1988.